SIZE EFFECT ON THE MECHANICAL PROPERTIES OF BCC TANTALUM NANOWIRES BY MOLECULAR DYNAMICS SIMULATIONS

Vildan GUDER

Department of Physics, Faculty of Science, Trakya University, 22030 Edirne, Turkey

Abstract

The size effect on the mechanical properties of body-centered cubic tantalum nanowires has been investigated by molecular dynamics simulations in which the interactions are expressed by the embedded atom method potential. The mechanical response of the nanowires with eight different thicknesses in the range of 2.3 nm and 9 nm with the same length has been examined by discussing the Elastic Modulus, yield stress, and neck strain. Radical differences have been observed in the mechanical properties of the nanosystem compared to its bulk counterpart. It is observed that the yield stress of tantalum nanowires decreases and approaches the bulk limit as the size increases while the Elastic Modulus increases to reach the bulk's value within the same size scale. The neck strain increases from 0.065 at 2.3 nm to 0.095 at 5 nm and oscillates around 0.09 for larger sizes than 5 nm.

Keywords: tantalum nanowires, mechanical properties, size effects, molecular dynamics simulation.

INTRODUCTION

With a chemical resistance comparable to noble metals, tantalum (Ta) is one of the metals with the highest corrosion resistance in natüre [1]. It is a tough, ductile metal, which can be formed into almost any shape. This feature allows it to be used as a coating material in the production of electronic components [2]. The extremely high cost of Ta-based materials restricts its industrial applications and causes studies to develop cost-effective systems. Therefore, there is a potential for increased use of Ta in the future [1]. Ta is a model element for the body-centered cubic (bcc) lattice due to its high phase stability even under external factors such as high pressure and temperature [3]. This feature has led researchers to examine the plastic and elastic properties of Ta and Ta based alloys [4]. Haskins et al. [5] examine the mechanical and relative thermodynamic stability of different phases at high temperatures and pressures in Ta using density functional theory-based model generalized pseudopotential theory. In the systematic study of Shang et al. [6], they discussed the phase stability of pure single crystal elements including Ta and observed a face-centered cubic (fcc) - hexagonal close-package (hcp) transition at 67.5 and 285 GPa by using the projector-augmented wave method and the generalized gradient approximation. Pan et al. [7] studied the tensile deformation of nanocrystalline Ta by using molecular dynamics (MD) simulations and showed that stress-induced phase transformation from bcc to fcc and hcp structures occurs locally, and high strain rate delays the transition. On the experimental side, it was reported a transformation of the physical phase from bcc to hexagonal-ω at high temperature is due to internal stress [8]. Recently, Florando et al. [9] investigated the effect of the conditions of uniaxial stress and laser-induced shock loading on twinning in Ta. They concluded that once twinning begins, it can grow as a function of stretching.

The aim of this work is to investigate the mechanical properties of single bcc crystalline Ta nanowires (NW) from a local perspective. For this purpose, the MD simulation method is used to understand the elastic and plastic responce of bcc Ta. The obtained results showed that the interatomic potential used in

the study is sufficient and reliable to understand the mechanical properties of Ta element. It is planned to extend this study to perform MD simulations of the uniaxial tensile deformation of nanocrystalline and polycrystalline Ta.

EXPOSITION

Large – Scale Atomic-Molecular Massively Parallel Simulator (LAMMPS) [10] was used to understand the deformation mechanism of bcc Ta NWs. MD simulations of Ta NWs were performed by using an interatomic potential of embedded atom method (EAM) [11].

It is well-known that the success of MD simulations is highly dependent on the correct description of the interactions between atoms. The reliability of the EAM potential used in the study was tested by comparing the known physical properties of cohesive energy and lattice constant for bulk Ta. For this purpose, the initial configuration of simulations was composed of the ideal bcc lattice with 16000 Ta atoms. The bulk system was subjected to energy-minimization procedure by the conjugate gradient algorithm. Table 1 lists the results of this test simulation for bcc Ta along with the available experimental and ab initio MD data. The reliability of EAM potentials used in MD simulations can be observed from the agreement of results between simulated and experimental/ab initio MD data.

Table 1. *The calculated lattice constant and cohesive energy values for Ta.*

	This work	**Exp.**
a (Å)	3.29	3.30[a,b]
E (eV/atom)	-8.10	-8.10[b]

[3][a], [13][b]

Table 2. *Supercell for bulk and NW systems and atomic numbers corresponding to this supercell.*

System	**Supercell (xa_o^3)**	**Atomic Number**
Bulk	20x20x20	16000
2.3 nm	7x7x50	4900
3.3 nm	10x10x50	10000
4 nm	12x12x50	14400
5 nm	15x15x50	22500
6 nm	18x18x50	32400
7 nm	21x21x50	44100
8 nm	24x24x50	57600
9 nm	27x27x50	72900

Prior to loading, all systems were relaxed using a constant number of the atom, volume, and energy (NVE) ensemble constraints for 10000 MD steps with a 0.001 ps time interval. While the constant number of atoms, volume and temperature (NVT) ensemble was used for the simulations of tensile loading of Ta NWs, the constant atomic number, pressure, and temperature (NPT) ensemble was used for the bulk case. To experience the effect of size, NWs of eight different thicknesses ranging from 2.3 nm to 9 nm were used, where the length of all NW is 16.5 nm. Table 2 lists the dimensions and atomic numbers of bulk and nano systems.

The NW model used in the tensile process is as follows. The NW was divided into two parts consisting of rigid (green spheres) and free atoms (red spheres). At both ends, which corresponds to 20% of the entire length of the NW, the rigid atoms were not allowed to interact with each other. The free atoms in the middle part could interact and could freely shrink or expand under the interatomic force. Periodic boundary conditions were used along the z axial direction while free boundary conditions were applied along the other two directions (x and y) during tensile deformation. The top and side view of model system studied in this work is shown in Fig. 1. All systems were subjected to a 25% tensile load along the z-axis using a strain rate of 0.001 ps^{-1} at 300 K.

Stress-strain curves obtained during tensile deformation are used to get information about the mechanical properties of the material. Fig. 2 shows that stress-strain curve for bulk and NW systems. For the early stage of tensile load, all curves in a region known as elastic increase linearly up to a certain strain value. After the elastic deformation, the stress reaches the maximum value with a different slope and drops sharply in the plastic region. Then the stress exhibits a zigzag behavior with increasing dislocations. It is observed from Fig.2 that the initial stress of the bulk system without any surface is very close to zero reflecting that it is fully relaxed. For NWs, the value of initial stress increases with decreasing size. This indicates that initial surface stress becomes an important factor for systems with a large surface-to-volume ratio. In addition,

the tensile value, where a sharp decrease is observed, also shifts towards larger values as the size increases. This result indicates that Ta NWs will withstand wider plastic deformation with increasing size.

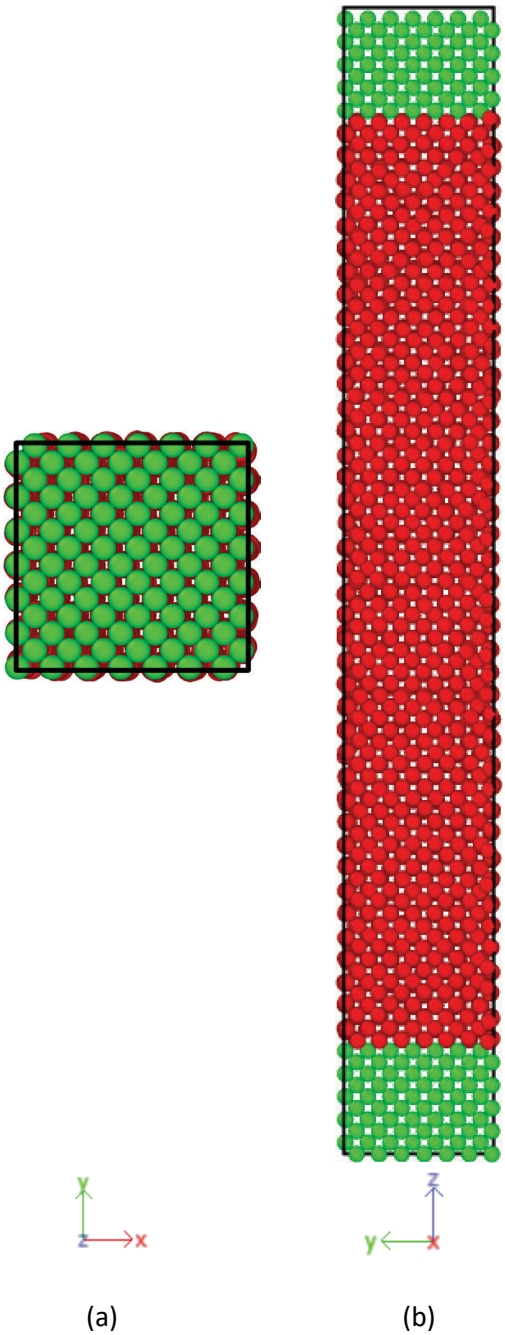

Fig. 1. *Atomistic model for Ta NWs. The top view of (a) all (b) The green and red spheres represent rigid and free atoms.*

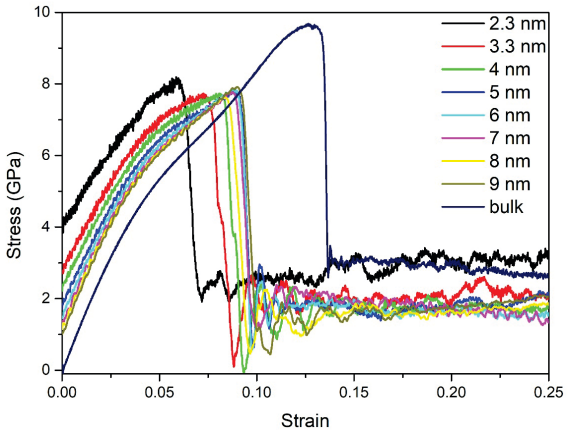

Fig. 2. *Dimension dependence of stress – strain relation in the tension process at strain rate of 0.001 ps^{-1} and 300 K.*

The mechanical properties such as yield stress, Elastic Modulus and neck strain as a function of strain extracted from curves plotted in Fig. 2 were displayed in Fig 3-5, respectively. In this study, the yield stress shown in Fig.3 was taken as the value of stress corresponding to the 0.05 strain. The yield stress determined for the bulk system is 5.3 GPa. It is observed that the yield stress of Ta NWs decreases with increasing size, starting from 7.66 GPa and approaching the bulk limit.

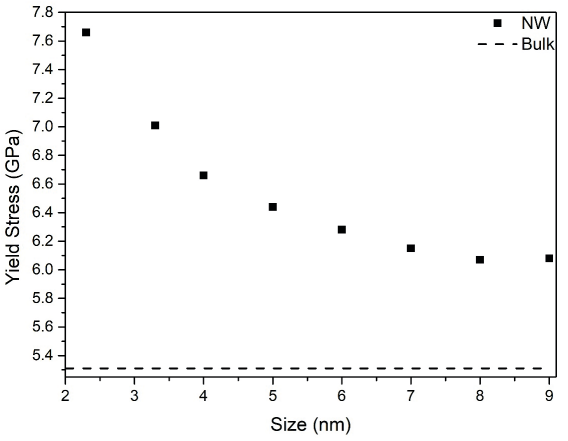

Fig. 3. *Size dependent relation of yield stress at strain rate of 0.001 ps^{-1} and 300 K.*

The Elastic Moduli for Ta NWs depicted in Fig. 4 were calculated from the tangent of the stress-strain curves within the strain value up to 0.01. The value of it for the bulk Ta is calculated as 143 GPa and this value is in agreement with the experimental data (186 GPa [7]). It is observed that the Elastic Modulus of Ta NWs increases and approaches the bulk limit as the size increases.

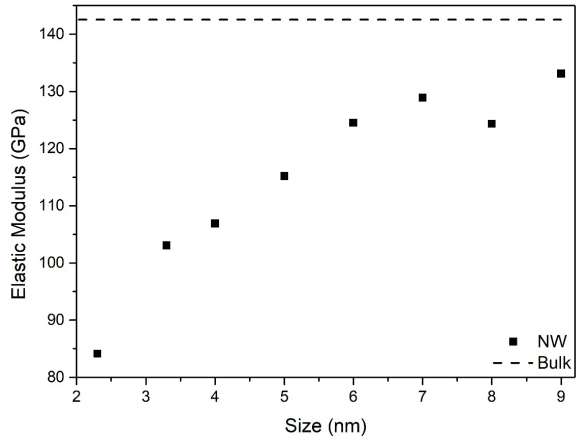

Fig. 4. *Size dependent relation of Elastic Modulus at strain rate of 0.001 ps^{-1} and 300 K.*

Fig. 5 shows that size dependent relation of neck strain at strain rate of 0.001 ps^{-1} and 300 K. The transition from elastic deformation to plastic one is observed in the system with the onset of the first dislocations. As a result of this situation, the atoms move out of their positions, the planes slip on each other and a neck is formed. The strain value at which a sharp decrease in stress is observed is called neck strain. The neck strain increases from 0.065 at 2.3 nm to 0.095 at 5 nm and oscillates around 0.09 for larger sizes than 5 nm.

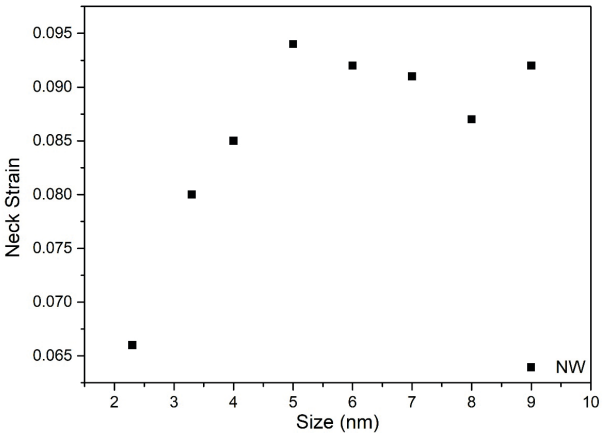

Fig. 5. *Size dependent relation of neck strain at strain rate of 0.001 ps^{-1} and 300 K.*

Simulation images taken during loading can be a guide for a clear view of yielding and neck formation during tensile simulation. From these images, visual information about the progress and spread of the deformation can be obtained. Fig. 6 (a–d) show snapshots from MD simulations corresponding to strains of initial, yield limit, neck and after the neck for 2.3 nm and 7 nm NW NWs at 300 K and strain rate 0.001 ps^{-1}, respectively, during tensile deformation. Fig. 6 (a) displays that the system has almost no stress after equilibration (before loading) and atoms are located at regular lattice points. In the Fig. 6 (b), the tensile load propagates and yields homogeneously in the system with increasing strain and this corresponds to the elastic deformation limit. The neck formation with increasing intensity of dislocations has been observed in Fig. 6 (c). The cross-sectional area of the NW decreases as the stress required for the elongation of the system is reduced. Then, the neck is formed. In Figure 6 (d), it is seen that this neck becomes more prominent with increasing strain as the dislocations move out free surface and multiple splits appear.

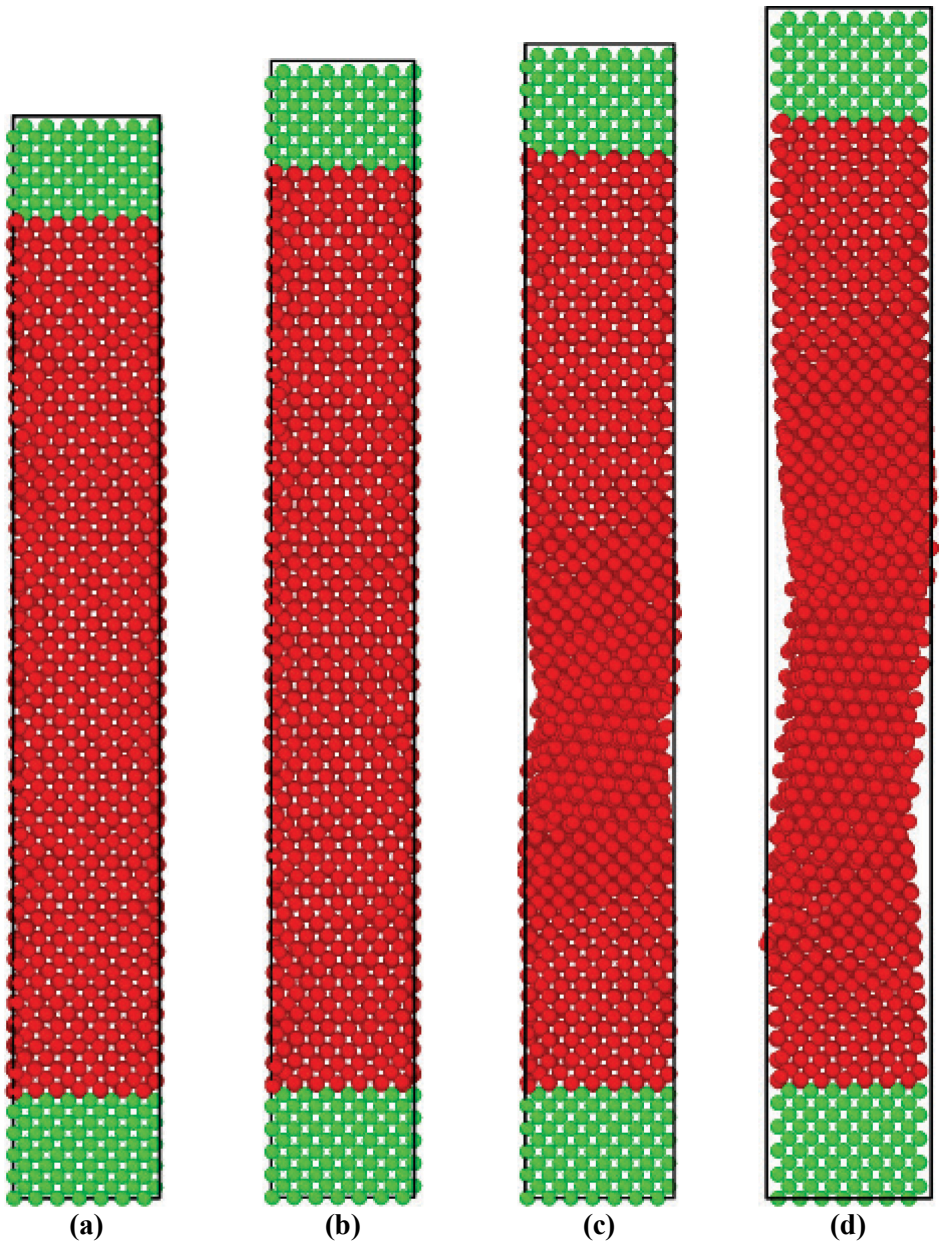

Fig. 6. *MD simulation snapshots at the strains of (a) 0, (b) 0.05, (c) 0.066, (d) 0.10 for 2.3 nm Ta NW.*

CONCLUSION

The uniaxial tensile deformation of Ta NWs with eight different thicknesses in the range of 2.3 nm and 9 nm has been investigated by the MD simulations. It is observed that the EAM potential used to describe interactions between Ta atoms is successful and reliable to predict ground state properties of Ta. The mechanical response of Ta NWs to tensile load under up to 25% deformation was investigated by with stress-strain curves. It is observed that Ta NWs shows great ductility up to 25% elongation. The yield stress of the thinnest NW considered here is 7.66 GPa, and it decreases with increasing size towards the value of bulk system (5.3 GPa). The Elastic Modulus for the bulk Ta is extracted from the stress-strain curves as 143 GPa. It has been observed that the Elastic Modulus is size dependent and increases with increasing size.

It is planned to extend this study to the investigate of twinning and/or phase transition that may occur in single and/or polycrystalline Ta NWs using different strain rates.

REFERENCES

[1] S.D. Cramer, B.S.J. Covino, eds., Corrosion of Tantalum and Tantalum Alloys, in: ASM Handb., ASM International, 2005: pp. 337–353.

https://doi.org/10.31399/asm.hb.v13b.a0003825.
[2] M. Alishahi, F. Mahboubi, S.M. Mousavi Khoie, M. Aparicio, E. Lopez-Elvira, J. Méndez, R. Gago, Structural properties and corrosion resistance of tantalum nitride coatings produced by reactive DC magnetron sputtering, RSC Adv. 6 (2016) 89061–89072. https://doi.org/10.1039/C6RA17869C.
[3] S.R. Chen, G.T. Gray, Constitutive behavior of tantalum and tantalum-tungsten alloys, Metall. Mater. Trans. A. 27 (1996) 2994–3006. https://doi.org/10.1007/BF02663849.
[4] C.-H. Lu, E.N. Hahn, B.A. Remington, B.R. Maddox, E.M. Bringa, M.A. Meyers, Phase Transformation in Tantalum under Extreme Laser Deformation, Sci. Rep. 5 (2015) 15064. https://doi.org/10.1038/srep15064.
[5] J.B. Haskins, J.A. Moriarty, R.Q. Hood, Polymorphism and melt in high-pressure tantalum, Phys. Rev. B. 86 (2012) 224104. https://doi.org/10.1103/PhysRevB.86.224104.
[6] S.L. Shang, A. Saengdeejing, Z.G. Mei, D.E. Kim, H. Zhang, S. Ganeshan, Y. Wang, Z.K. Liu, First-principles calculations of pure elements: Equations of state and elastic stiffness constants, Comput. Mater. Sci. 48 (2010) 813–826. https://doi.org/10.1016/j.commatsci.2010.03.041.
[7] Z. Pan, Y. Li, Q. Wei, Tensile properties of nanocrystalline tantalum from molecular dynamics simulations, Acta Mater. 56 (2008) 3470–3480. https://doi.org/10.1016/j.actamat.2008.03.025.
[8] L. Burakovsky, S.P. Chen, D.L. Preston, A.B. Belonoshko, A. Rosengren, A.S. Mikhaylushkin, S.I. Simak, J.A. Moriarty, High-Pressure—High-Temperature Polymorphism in Ta: Resolving an Ongoing Experimental Controversy, Phys. Rev. Lett. 104 (2010) 255702. https://doi.org/10.1103/PhysRevLett.104.255702.
[9] J.N. Florando, B.S. El-Dasher, C. Chen, D.C. Swift, N.R. Barton, J.M. McNaney, K.T. Ramesh, K.J. Hemker, M. Kumar, Effect of strain rate and dislocation density on the twinning behavior in tantalum, AIP Adv. 6 (2016) 045120. https://doi.org/10.1063/1.4948528.
[10] S. Plimpton, Fast Parallel Algorithms for Short-Range Molecular Dynamics, J. Comput. Phys. 117 (1995) 1–19. https://doi.org/10.1006/jcph.1995.1039.
[11] A. Agrawal, R. Mishra, L. Ward, K.M. Flores, W. Windl, An embedded atom method potential of beryllium, Model. Simul. Mater. Sci. Eng. 21 (2013) 085001. https://doi.org/10.1088/0965-0393/21/8/085001.
[12] http://www.webelements.com/tantalum/crystal_structure.html, (n.d.).
[13] C. Kittel, Introduction to Solid State Physics, New York: John Wiley & Sons Inc., 1986.
[14] Y. Pan, W.M. Guan, K.H. Zhang, First-principles calculation of the phase stability and elastic properties of ZrPt compounds at ground state, Phys. B Condens. Matter. 427 (2013) 17–21. https://doi.org/10.1016/j.physb.2013.05.039.